PHYSICAL REVIEW E **96**, 020901(R) (2017)

Transport analogy for segregation and granular rheology

Siying Liu and Joseph J. McCarthy*
Department of Chemical and Petroleum Engineering, University of Pittsburgh, Pittsburgh, Pennsylvania 15261, USA
(Received 13 January 2017; revised manuscript received 26 April 2017; published 10 August 2017)

Here, we show a direct connection between density-based segregation and granular rheology that can lead to insight into both problems. Our results exhibit a transition in the rate of segregation during simple shear that occurs at $I \sim 0.5$ and mimics a coincident regime change in flow rheology. We propose scaling arguments that support a packing fraction criterion for this transition that can both explain our segregation results as well as unify existing literature studies of granular rheology. By recasting a segregation model in terms of rheological parameters, we establish an approach that not only collapses results for a wide range of conditions, but also yields a direct relationship between the coordination number z and the segregation velocity. Moreover, our approach predicts the precise location of the observed regime change or saturation. This suggests that it is possible to rationally design process operating conditions that lead to significantly lower segregation extents. These observations can have a profound impact on both the study of granular flow or mixing as well as industrial practice.

DOI: 10.1103/PhysRevE.96.020901

Segregation [1] is a costly phenomenon that has garnered research for decades [2–4]. In contrast, the study of dense phase granular rheology has only recently gained traction, but significant inroads have been made [5–11]. Despite these parallel strides, only a tenuous connection has been proposed [12] between these two seemingly disparate topics and work focusing on building a formal analogy is lacking, despite the synergistic advantages that analogies have afforded [13] in a variety of fields [14–17].

It is generally accepted [18–20] that the scaling of gravity-driven density segregation is proportional to the density difference between species as well as to the local value of the shear rate within the flow (although segregation in the absence of gravity has been shown to be more complex [21,22]). This simple phenomenological scaling results in just three relevant dimensionless groups—for segregation velocity, $\bar{v}_s = v_s/(\sqrt{g d_p})$, shear rate, $\bar{\gamma} = \dot{\gamma}\sqrt{d_p/g}$, and density, $\bar{\rho} = \rho_h/\rho_l$, where g is the acceleration due to gravity and d_p is the particle diameter; however, it does not account for the impact of varying boundary conditions (specifically, confining pressure P), thus it does not readily allow direct coupling between granular flow rheology and the segregation rate. In this Rapid Communication, we examine a simplified "ideal solution" segregating flow whereby isolated dense intruders segregate as a function of a host of rheological variables. By explicitly accounting for the confining pressure, we make a more direct connection between rheology and segregation. In this way, we not only shed light on how rheological-segregation coupling may be modeled, but also uncover a direct analogy between measurements of rheological variables and the resulting segregation rate.

A recent survey of density-based segregation models [23] found that a successful phenomenological model for the density-driven segregation velocity has been set forth by Tripathi and Khakhar [19]. They begin with a force balance on a single dense particle in a medium of light particles to get

$$0 = F_w - F_b + F_d, \tag{1}$$

where F_w is the weight of the dense particle, F_b is the buoyant force, and F_d is the particle drag force. Taking the particle drag force to have a Stokesian form, they assume

$$F_d = \beta \pi \eta d_p v_s, \tag{2}$$

where η is the particle medium viscosity, d_p is the particle diameter, β is a constant, and v_s is the segregation velocity. Assuming that the drag force and net particle weight are in balance, after simplification, yields an expression for v_s which may be written as

$$v_s = \frac{g d_p^2(\rho_h - \rho_l)}{6\beta\eta}, \tag{3}$$

where g is the acceleration due to gravity and ρ_i is the density of the heavy (h) and light (l) particles, respectively. In order to recover the previously mentioned traditional scaling, one assumes that the stress τ within the granular flow is shear rate independent so that we can write

$$\eta = \frac{\tau}{\dot{\gamma}} \propto \frac{1}{\dot{\gamma}}. \tag{4}$$

Based on the above equations, we recover that (1) v_s is proportional to the shear rate $\dot{\gamma}$, and (2) at a constant shear rate the segregation velocity v_s should scale as $(\rho_h - \rho_l)$.

To test these predicted scaling relations, yet at the same time allow for the variation of flow boundary conditions, we employ the discrete element method (DEM) to examine a wall-driven periodic plane shear cell. The details of the model can be found in a previous paper from our group [24]. Table I shows the material properties that were used in the simulations reported here. A schematic of the simulated three-dimensional (3D) plane shear flow system is shown in Fig. 1. Periodic boundaries are used in both the x and z directions. In most trials, the majority of the particles have the same (light) density of $\rho_l = 1300\ \mathrm{kg/m^3}$, material properties that roughly match cellulose acetate, and an average radius of 4.5 mm with a 10% particle size distribution to prevent crystallization. In some cases we examine the impact of varying particle diameter over a range from $d_p = 6.0$ to 18 mm in 3.0 mm increments. For all simulations, eight uniform heavy intruders (which

*jjmcc@pitt.edu

TABLE I. Material properties used in the simulations.

Parameter	Acetate	Glass	Steel
Young's modulus E (GPa)	2.9	68.95	193
Density ρ (kg/m^3)	1300	2700/3900	7900
Coefficient of friction μ	0.3	0.3	0.3
Poisson ratio ν	0.43	0.33	0.29
Yield stress σ_y (MPa)	30	68.95	265

have the same radius as the light particles, but with varying heavy density ρ_h) are randomly placed in the system. Three different ρ_h values are used (2700, 3900, and 7900 kg/m^3), along with corresponding material properties that roughly match glass, "heavy glass," and stainless steel, respectively. The top and bottom walls (shown as black in Fig. 1) are roughened with particles and the top wall is given varying masses in order to examine the effect of confining pressure (P). Alternatively, several trials were run at a constant volume fraction (i.e., fixed height h) where we measured the time average of the pressure at the top wall (rather than prescribing the confining pressure). Shearing velocity is varied from 0.1 to 4.0 m/s (0.1, 0.5, 1, 2, 3, and 4 m/s) while the bottom wall remains static. To obtain a nearly homogeneous shear flow, fins made of wall particles are attached to both the top and bottom walls, and in most simulations we employ a modified gravitational field whereby (net) gravitational forces act only on the heavy intruders (similar to the approach of Ref. [25]). The particle bed is deep enough (15 particle diameters) that the segregating intruders reach a steady segregation velocity under all examined conditions. In a small number of simulations full gravity effects are included, however, due to shear localization in these cases we perform all calculations based on the local value of the shear rate (and only measure the segregation velocity while in the sheared region).

In Fig. 2 we show the dimensionless segregation velocity obtained for the average of the heavy intruders for three different density ratios under a range of boundary conditions (confining pressures versus fixed volumes and our modified

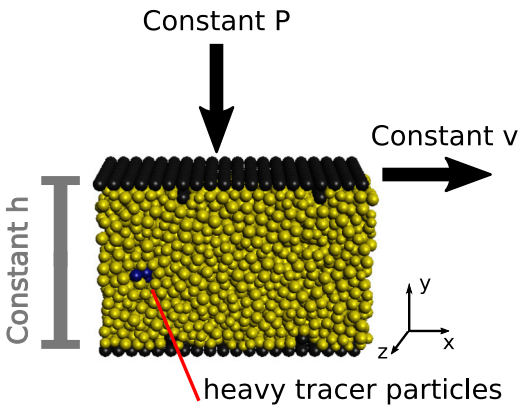

FIG. 1. Schematic of the simulated plane shear geometry. The 3D flow is periodic in both the streamwise (x) and transverse (z) directions. Blue (dark) particles are heavy intruders while yellow (light) particles are lower density particles. We employ either constant pressure or constant volume boundary conditions.

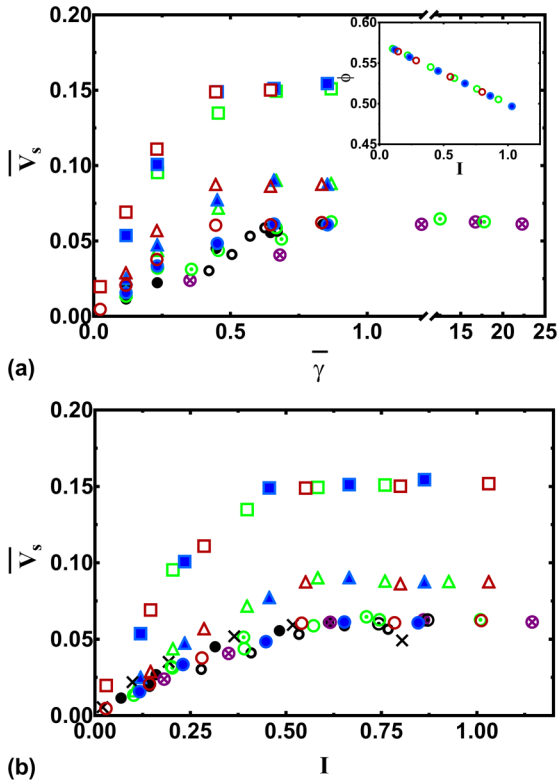

FIG. 2. Segregation velocity under varying conditions of shear rate, density ratio, particle diameter, and boundary conditions. Differing colors represent boundary conditions [constant pressures: 78 Pa, red (dark gray); 117 Pa, blue (solid light gray); 156 Pa, green (open light gray); constant volume, solid circles; full gravity effects, dotted and crossed circles] while shape represents the density ratio (circle, $\bar{\rho} = 2$; triangle, $\bar{\rho} = 3$; square, $\bar{\rho} = 6$). While most particles are 9.0 mm in diameter, the thick-walled open circles represent a range from 6.0 to 18.0 mm. (a) The dimensionless segregation velocities are plotted vs the shear rate made dimensionless with $\sqrt{g/d_p}$. The inset shows packing fraction as a function of I. (b) In this panel we have replotted the $\bar{v}_s$ as a function of inertia number (I). Note that the varying boundary conditions all collapse onto individual curves corresponding to different density ratios. In all figures, error bars on the data are smaller than the symbol sizes chosen.

gravity field versus full gravity), particle diameters, and shear rates. In Fig. 2(a), which shows the variation of $\bar{v}_s$ with dimensionless shear rate ($\bar{\gamma}$), we note that there are roughly three groups of curves, corresponding to each of the three density ratios; however, it is clear that there are a number of issues with this naive scaling. First, there is a systematic variation in the value of $\bar{v}_s$ for differing boundary conditions, whereby higher pressures and/or the constant volume cases result in a routinely smaller value of the segregation velocity. Second, when varying the particle diameter, we notice a qualitatively different shape to the scatter plot (it does not appear to pass through the origin, for example). Finally, when including the full effects of gravity, our segregation velocity values are uniformly lower than for the corresponding shear rates in modified gravity cases, and ultimately the segregation rate saturates at dramatically larger values of the dimensionless shear rate.

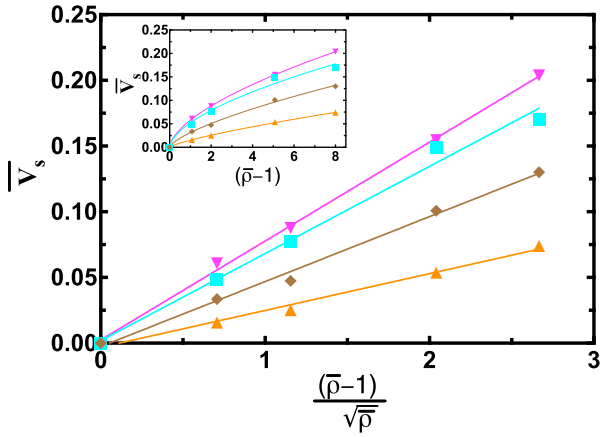

FIG. 3. Variation of dimensionless segregation velocity with varying density at fixed values of the inertia number (upright triangle, $I = 0.1193$; diamond, $I = 0.2350$; square, $I = 0.4563$; inverted triangle, $I = 0.8627$). The inset shows the traditional scaling of the segregation rate with the dimensionless density difference. Note that, in contrast to previous studies, we find a power-law relationship with exponents that range from 0.6 to 0.75. In contrast, when we plot the segregation velocity vs our proposed density scaling, we obtain straight lines.

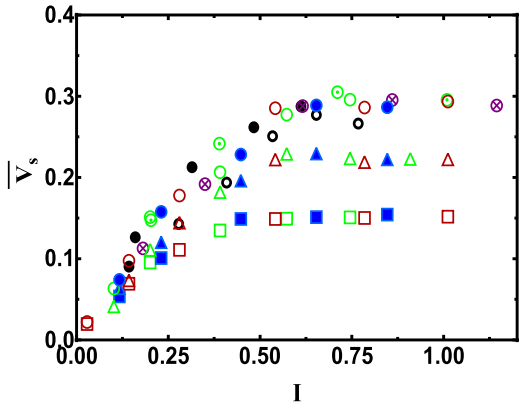

FIG. 4. Traditional scaled segregation velocity under varying conditions of shear rate, density ratio, particle diameter, and boundary conditions. Differing colors represent boundary conditions [constant pressures: 78 Pa, red (dark gray); 117 Pa, blue (solid light gray); 156 Pa, green (open light gray); constant volume, solid circles; full gravity effects, dotted and crossed circles] while shape represents the density ratio (circle, $\bar{\rho} = 2$; triangle, $\bar{\rho} = 3$; square, $\bar{\rho} = 6$). While most particles are 9.0 mm in diameter, the thick-walled open circles represent a range from 6.0 to 18.0 mm. The dimensionless segregation velocities are plotted vs the shear rate made dimensionless with $\sqrt{g/d_p}$. The magnitude of the segregation velocity is scaled by the traditional density scaling [that is, $(\rho_h/\rho_l - 1)$]. Note that, particularly in the saturated rate region, it is clear that this scaling does not collapse the data.

In order to fix these issues with the scaling, and as a first step toward connecting segregation to granular rheology, in Fig. 2(b) we instead plot $\bar{v}_s$ against a different dimensionless shear rate, that of the inertia number (I). The inertia number [5], given as $I = \dot{\gamma} d_p \sqrt{\frac{\rho}{P}}$, is the final, relevant independent dimensionless group governing this problem; it relates the time scale of shearing to the time scale of consolidation, and has been a staple of constitutive model development in recent years [8–11]. We note that I is a better independent variable for correlating changes in segregation velocity as the scatter from pressure (and constant volume) variation is now eliminated in the higher density ratio (triangle and square) trials. Moreover, the low density ratio (circle) case now collapses results not only for varying boundary conditions, but also for varying particle diameters and for both full and modified gravity cases (note that the modified gravity case uses the measured average bed pressure and the local shear rate in the calculation of I). Using the inertia number allows us to capture a clear observation that the segregation rate saturates [Fig. 2(b)] at a specific value of I in much the same way that the effective friction (μ_{eff}) is seen to saturate (at high inertia numbers) in $\mu_{\text{eff}}(I)$ rheology [5,26]. Also, we note that, while our $\bar{v}_s$ results now collapse onto three curves regardless of particle size and boundary condition, the relevant scaling for the density ratio is not captured in this plot. This scaling is examined next.

Turning to the impact of the density ratio, one can note that using the traditional density scaling suggested from Eq. (3) $(\rho_h/\rho_l - 1)$ fails to collapse the data [that is, the plot in Fig. 3 (inset) does not lead to a straight line and Fig. 4 does not collapse, especially on the saturated regime]. If we relax the assumption that all segregating flows operate in the rate-independent regime and instead develop a scaling relation for the local viscosity near a segregating particle, we can recast Eq. (3) and not only recover the proper density relationship (Fig. 3, motivated below), but also establish a direct analogy between granular flow rheology and the segregation velocity.

We start by choosing a characteristic stress scale in the neighborhood of the heavy intruder(s) as the quantity $\tau_{\text{char}} \sim \rho_h g d_p$. If we similarly take the local shear rate to be related to a characteristic collisional velocity v_{coll} (to be identified later), divided by the particle diameter, we obtain

$$\eta \sim \frac{\rho_h g d_p}{v_{\text{coll}}/d_p}. \tag{5}$$

For a heavy intruder, a density dependence of the collisional velocity v_{coll} arises due to the fact that the intruder must undergo repeated collisions with the lighter "background" particles. By performing a conservation of energy balance around a colliding particle [27], we obtain a postcollision characteristic velocity given as $v_{\text{coll}} \sim v_o(\frac{\rho_h}{\rho_l})^{1/2}$, where v_o may be thought of as the precollisional characteristic velocity. Combining these expressions, we can write an equation for the viscosity near a heavy intruder particle that is segregating within a granular fluid as

$$\eta \sim \frac{\rho_h g d_p^2}{v_o\left(\frac{\rho_h}{\rho_l}\right)^{1/2}}. \tag{6}$$

This simple model suggests a modification of the density scaling from what is traditionally used whereby

$$v_s \sim \frac{v_o(\bar{\rho} - 1)}{\sqrt{\bar{\rho}}}. \tag{7}$$

As a direct test of this scaling, we plot the measured segregation velocity as a function of this density scaling for fixed values

of the inertia number (see Fig. 3). Note that each set of results examined lies on a straight line whose slope is a function of the inertia number chosen and that all curves correctly pass through the origin.

In order to more fully realize the form of Eq. (7), we finally examine the characteristic (pre)collisional velocity v_o. Obviously, in the absence of interactions with neighboring particles, the characteristic velocity of a falling intruder would scale as $\sqrt{d_p g}$ (motivating the choice of dimensionless scaling thus far used). If we argue that the relevant velocity is actually a "frustrated free fall" whereby the characteristic velocity varies from this scaling value solely due to interactions with neighboring particles, we can write that the number of interactions with neighbors per unit time is captured by the product of the coordination number z and the shear rate, $z\dot{\gamma}$. That is, the quantity $z\dot{\gamma}$ may be thought of as the inverse of the time between interparticle interactions (note that z has been shown to be a function of the inertia number [10,11] so that, at higher inertia numbers, the time between interactions increases). We note that, in our results, the average coordination number per particle decreases from a finite static value via a power law of the form $z \sim I^{-a}$—similar to what was discussed in Ref. [7]—however, as seen in Fig. 5(a), we find two regimes where $a = 1/3$ and 1 for I values below and above 0.5, respectively. We note that this transition point is coincident with the saturation location of both the effective friction coefficient μ_{eff} and the segregation velocity. Finally, if we limit the effective number of neighbor interactions to those that occur faster than the consolidation time scale, $t_c = d_p(\rho_l/P)^{1/2}$, we obtain a choice of v_o that is given by

$$v_o \sim (\sqrt{d_p g})z\dot{\gamma}t_c = (\sqrt{d_p g})zI. \tag{8}$$

One way to interpret our scaling in Eq. (8) is that the maximum time between collisions is the consolidation time. Thus, in the limit of large I, we obtain free-fall scaling during the full extent of the consolidation time. At the other extreme, where the time between collisions is small, the "frustrated free-fall" velocity can become quite small. Combining Eq. (7) with (8) and recovering the constants from previous equations yields an expression for the dimensionless segregation velocity as

$$\bar{v}_s = \frac{v_s}{\sqrt{d_p g}} = \frac{z(\bar{\rho}-1)}{6\beta\sqrt{\bar{\rho}}}I. \tag{9}$$

Thus, by using our scaling, and determining a relationship between the collision frequency and inertia number (I), we yield a closed form equation for segregation velocity that includes only a single parameter β that captures the drag force felt on a segregating particle [as well as an $O(1)$ correction to our collision velocity scaling argument]. Figure 5(b) shows the relationship between segregation velocity (scaled with our density relation) and I for all simulation conditions studied and includes a line corresponding to Eq. (9) with $\beta = 1$ (which, in a fluid system, would imply that form drag is small compared to frictional drag).

It is interesting to note that the location of the segregation velocity (and μ_{eff} and z) transition corresponds to the value of I where the solid packing fraction decreases below a value of roughly $\phi \approx 0.52$ [Fig. 2(a) inset]. This value of the packing fraction is characteristic of a simple cubic lattice of equal sized

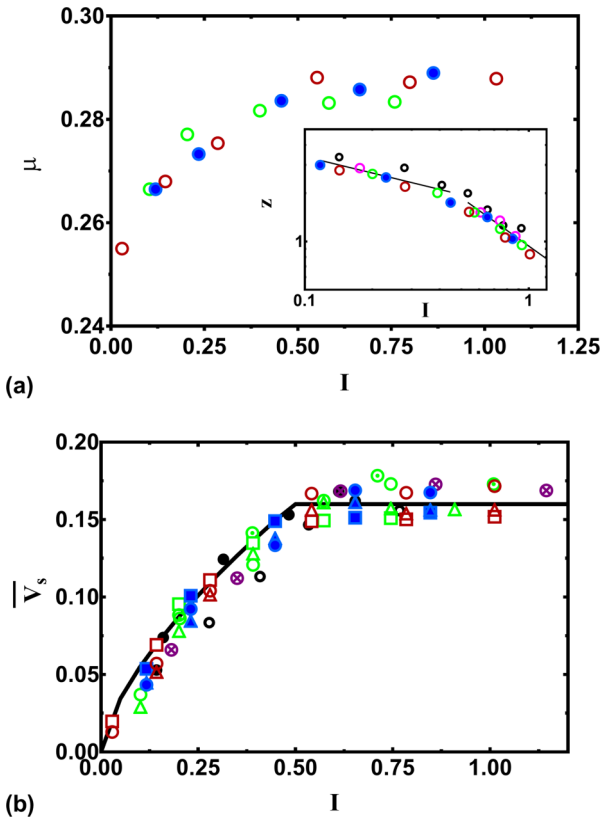

FIG. 5. Rheology and segregation in a sheared cell system under varying conditions of shear rate, density ratio, particle diameter, and boundary conditions (symbols explained in Fig. 2). (a) shows how the effective friction coefficient changes with the inertia number. The inset shows the variation of the coordination number with I. Note that both rheological quantities display a regime change near a value of $I = 0.5$. (b) shows the dimensionless segregation velocity rescaled with our proposed density scaling [Eq. (7)] and plotted against I. Note that all results fall on a master curve regardless of gravitational condition, boundary condition, or other process parameters. The included line represents the model proposed in Eq. (9). The inset shows the packing fraction as a function of I.

spheres. While the rheological transition from linear $\mu_{\text{eff}}(I)$ to saturated μ_{eff} has been reported at varying values of I in the literature [5,7,10], examining these transitions in light of this packing fraction observation one notes that a simple cubic solids' fraction criterion would identify this critical I value irrespective of whether the system is 2D [5,6] or 3D [10]. Regardless of the origin of this transition, here we show that recasting our data in light of the inertia number collapses our results onto a single master curve for a wide variety of process variables, boundary conditions, and gravitational conditions and allows us to recognize—and predict the location of—a regime where the segregation rate saturates. This observation could have significant industrial importance as it could enable the rationale design of industrial processing methods that could lead to dramatically reduced segregation extents since operating in the "saturated" regime (i.e., at high I values) will enable more rapid processing to reduce the ultimate degree of segregation observed. Moreover, this work highlights that density-based segregation is not only coupled to the underlying flow rheology in shearing geometries, but that a true analogy exists

whereby determination of the relationship between the coordination number (z) and I can lead directly to a quantitative expression for the segregation velocity (and likely vice versa).

We wish to acknowledge the support of the International Fine Particle Research Institute (IFPRI) for partial funding of this work.

[1] J. M. Ottino and R. M. Lueptow, On mixing and demixing, Science **319**, 912 (2008).
[2] R. L. Brown, The fundamental principles of segregation, The Inst. Fuel **13**, 15 (1939).
[3] J. C. Williams, The segregation of powders and granular materials, Fuel Soc. J. **14**, 29 (1963).
[4] J. M. Ottino and D. V. Khakhar, Mixing and segregation of granular materials, Annu. Rev. Fluid Mech. **32**, 55 (2000).
[5] G. D. R. Midi, On dense granular flows, Eur. Phys. J. E **14**, 341 (2004).
[6] P. Jop, Y. Forterre, and O. Pouliquen, A constitutive law for dense granular flows, Nature (London) **441**, 727 (2006).
[7] F. da Cruz, S. Emam, M. Prochnow, J.-N. Roux, and F. Chevoir, Rheophysics of dense granular materials: Discrete simulation of plane shear flows, Phys. Rev. E **72**, 021309 (2005).
[8] K. Kamrin and G. Koval, Nonlocal Constitutive Relation for Steady Granular Flow, Phys. Rev. Lett. **108**, 178301 (2012).
[9] E. Azéma and F. Radjaï, Internal Structure of Inertial Granular Flows, Phys. Rev. Lett. **112**, 078001 (2014).
[10] R. C. Hurley and J. E. Andrade, Friction in inertial granular flows: Competition between dilation and grain-scale dissipation rates, Granular Matter **17**, 287 (2015).
[11] E. DeGiuli, J. N. McElwaine, and M. Wyart, Phase diagram for inertial granular flows, Phys. Rev. E **94**, 012904 (2016).
[12] F. Guillard, Y. Forterre, and O. Pouliquen, Scaling laws for segregation forces in dense sheared granular flows, J. Fluid Mech. **807**, R1 (2016).
[13] H. M. Jaeger and S. R. Nagel, Physics of the granular state, Science **255**, 1523 (1992).
[14] O. Reynolds, On the extent and action of the heating surface of steam boilers, Proc. Lit. Philos. Soc. Manchester **14**, 1 (1874).
[15] A. P. Colburn, Relation between mass transfer (absorption) and fluid friction, Ind. Eng. Chem. **22**, 967 (1930).
[16] I. R. Peters, S. Majumdar, and H. M. Jaeger, Direct observation of dynamic shear jamming in dense suspensions, Nature (London) **532**, 214 (2016).
[17] D. Bi, J. Zhang, B. Chakraborty, and R. P. Behringer, Jamming by shear, Nature (London) **480**, 355 (2011).
[18] D. V. Khakhar, J. J. McCarthy, and J. M. Ottino, Radial segregation of granular mixtures in rotating cylinders, Phys. Fluids **9**, 3600 (1997).
[19] A. Tripathi and D. V. Khakhar, Density difference-driven segregation in a dense granular flow, J. Fluid Mech. **717**, 643 (2013).
[20] H. Xiao, P. B. Umbanhowar, M. Ottino, and R. M. Lueptow, Modelling density segregation in flowing bidisperse granular materials, Proc. R. Soc. London, Ser. A **472**, 20150856 (2016).
[21] M. Y. Louge, J. T. Jenkins, H. Xu, and B. Ö. Arnarson, Granular segregation in collisional shearing flows, in *Mechanics for a New Millennium*, edited by H. Aref and J. W. Phillips (Springer, Dordrecht, 2001), pp. 239–252.
[22] Y. Fan and K. M. Hill, Shear-induced segregation of particles by material density, Phys. Rev. E **92**, 022211 (2015).
[23] S. Liu and J. J. McCarthy, Validating granular segregation rate models, AIChE J. **63**, 3756 (2017).
[24] S. T. Nase, W. L. Vargas, A. A. Abatan, and J. J. McCarthy, Discrete characterization tools for cohesive granular material, Powder Technol. **116**, 214 (2001).
[25] N. Khola and C. Wassgren, Correlations for shear-induced percolation segregation in granular shear flows, Powder Technol. **288**, 441 (2016).
[26] J. M. N. T. Gray and A. N. Edwards, A depth-averaged $\mu(I)$-rheology for shallow granular free-surface flows, J. Fluid Mech. **755**, 503 (2014).
[27] J. R. de Bruyn and A. M. Walsh, Penetration of spheres into loose granular media, Can. J. Phys. **82**, 439 (2004).